Long-Range Forecasting and Climate Research

An Interim Analysis of the Leading Covariance Eigenvectors of Worldwide Sea Surface Temperature Anomalies for 1901-80

by

C. K. Folland and A. Colman

[illegible] 20

April 1988

Meteorological Office (Met. O. 13)
London Road
Bracknell
Berkshire RG12 2SZ

ORGS UKMO L

National Meteorological Library
FitzRoy Road, Exeter, Devon. EX1 3PB

METEOROLOGICAL OFFICE
6 JUN 1988
152281
LIBRARY

JM

LRFC 20

AN INTERIM ANALYSIS OF THE LEADING COVARIANCE EIGENVECTORS OF WORLDWIDE SEA SURFACE TEMPERATURE ANOMALIES FOR 1901-80

C K Folland and A Colman

April 1988

Abstract

This is a preliminary report on some characteristics of the first three non-rotated covariance eigenvectors (EOFs) of worldwide seasonal sea surface temperature anomalies (SST) analysed in a 10° x 10° space scale. The Meteorological Office Historical Sea Surface Temperature Data Set (MOHSST) has been used to make the calculations. The EOFs have been calculated for separate three monthly seasons and for all seasons together for the period 1901-1980. Relationships are shown between EOFs 1-3 and global mean SST, SST in the tropical E Pacific and Sahel rainfall respectively. The EOFs are provisional as the corrections applied here to SST data for the predominant use of uninsulated sea temperature buckets prior to 1942 [Bottomley et al (1988), (1)] will be revised soon as results of research to be described in Folland and Parker (1989), (2) are available.

1. Introduction

1.1 SST data

The SST data used here are seasonal 10° x 10° anomalies taken from MOHSST3 (Meteorological Office Historical Sea Surface Temperature Data Set, version 3, (Bottomley et al (1988) (1), Parker (1987) (3)). For this analysis the data have been made "complete" for the shaded areas shown in Figure 1; thus SST anomalies (calculated from 1951-80 averages) have been interpolated where necessary in all seasons since 1901. A full description will appear elsewhere but, briefly, two forms of interpolation have been used:-

(a) spatial interpolation from observed or temporally interpolated SST anomalies in immediately adjacent 10° x 10° squares. Only data in the same season were used.

(b) time-wise interpolation of SST anomalies in a given 10° x 10° square using Chebyshev polynomials.

The results of (a) and (b) were weighted according to their estimated reliability and then combined. Thus an SST anomaly estimated using (b) and when there is no data observed for several seasons before or after the given season would have little weight unless it were the only estimate available. Anomalies exceeding ±3°C were not accepted in any 10° x 10° squares except in the region 10°N -10°S, 180°W to the S American coast where a limit of +4°C to -3°C was set. Interpolated anomalies were

restricted to ±2°C except in the above region where the limit was set to +3°C to -2°C. The four seasons are defined to be: Dec-Feb (winter), Mar-May (spring) etc.

1.2 SST anomaly Eigenvectors

Non-rotated EOFs have been used as the intention here is to explore the extent to which coherent, nearly worldwide, SST anomaly patterns can be found. Rotation is needed in future to determine the smaller scales of SST anomaly patterns and to check further the reality of some "worldwide" SST patterns. Covariance rather than correlation EOFs have been studied most because an important application of this research has been to seasonal tropical rainfall forecasting where it is desirable that absolute variations of SST should be represented.

A problem has been found with appropriately weighting the 10° x 10° areas prior to covariance EOF analysis. The SST anomaly data should be weighted in proportion to the square roots of the 10° x 10° areas to provide the correct areal weighting of covariances in the covariance matrix. When this weighting is done, the eigenvalues of EOF1 and EOF2 become similar in magnitude and the resulting SST anomaly patterns contained in EOF1 and EOF2 become confused (see Richman, 1986 (4)) and cannot be easily related to any physical quantity. If the data are not weighted, this problem disappears but there is a risk that the EOFs will represent real SST patterns less well. New corrections not yet completely worked out for the use of mostly uninsulated bucket prior to 1942 data might alleviate this problem. Tests suggest that the first three all seasons EOFs derived from weighted SST data that incorporate preliminary versions of the new bias corrections do have significantly different eigenvalues from one another and their spatial patterns are quite similar to those presented here. Use of unweighted SST anomaly data could artificially reduce (increase) the variance explained by EOF patterns that may be concentrated in the tropics (extratropics) and distort slightly the shape of EOF patterns that are genuinely important in both regions. This must be borne in mind when reading this paper.

1.3 Use of 10° x 10° regions

This size of region has been selected because it reduces the "noise" due to the poorer sampling of the 5° x 5° regions which are the basic units of MOHSST but retains most of the information contained in the smaller regions. Fig 2 shows sample simultaneous correlations between seasonal 10° x 10° anomalies (all seasons, multiplied by 100) calculated between the four selected shaded squares shown and those surrounding 10° x 10° squares that are placed within the solid lines. The correlations of the shaded areas with adjacent 10^{o} x 10^{o} squares are typically around .4 to .7 and tend to be higher in an east-west than in a north-south direction. Thus 10° x 10° is considered to be a reasonable size of square to use. Each square can be conveniently thought of as containing a "cluster" of SST anomalies whose characteristics are sufficiently similar to justify the use of the average anomaly calculated over the square to represent temporal variations of SST anomalies in the square.

2. RESULTS

2.1 All seasons SST anomaly EOFs

Table 1 summarises the main statistical characteristics of the first ten all seasons EOFs. The last column gives the results of a test devised by North et al (5) to determine whether successive eigenvectors have statistically distinct eigenvalues (at the 95% confidence level). The set of all-seasons EOFs are well-behaved in this respect.

Figs 3a-5a show the patterns of weights for EOFs 1-3 while Figs 3b-5b give their time series plotted against a physical parameter with which they are associated. The EOF weights have been multiplied by 1000. The relationship between the EOF weights and the EOF time series Z_{kt} is:-

$$Z_{kt} = 10^{-3} \left(\sum_{i=i}^{2944} w_{ki} \, s_{it} \right) \qquad (1)$$

where t = season t, i = ith 10° x 10° square and k = kth EOF. Z_{kt} is the time coefficient, w_{ki} is weight of the kth EOF in the ith 10° x 10° square and s_{it} is the value of the SST anomaly in 10° x 10° square i at time t. The "contribution" of EOF k to an SST anomaly at position i is

$$s'_{it} = 10^{-3}(w_{ki} \, s_{it}) \ °C \qquad (2)$$

where s'_{it} is the SST anomaly estimated from EOF k only. For diagnostic purposes we can partly overcome the problem of having to use "unweighted" eigenvectors by calculating

$$Z'_{Kt} = 10^{-3}(a_i \, w_{ki} \, s_{it}) \qquad (3)$$

where a_i are additional weights proportional to the area of each 10° x 10° square. The Z'_k time series are no longer uncorrelated but Z'_k should be better correlated with physical quantities derived from weighted averages of 10° x 10° SST values (such as global mean SST). Table II shows selected correlations between EOFs 1-3 and physical quantities using Z_K and Z'_K.

For the period 1901-87, correlations significant at the 99% confidence level in Table II are shown starred. Bartlett's (1935) (6) technique was used to make a crude estimate of the number of degrees of freedom for the correlations though non-stationarity of the series makes the estimates imprecise. For correlations with EOF1 (all versions) 8 degrees of freedom were estimated; for correlations involving EOF2, 100 degrees of freedom were estimated (this is especially uncertain) and for correlations including EOF3, 25 degrees of freedom were estimated.

EOF1 clearly represents seasonal global mean SST back to 1856, (Fig 3b), ie well before the period (1901-80) for which EOF1 was calculated. As expected, Z'_1 gives slightly higher correlations than does Z_1. EOF1 has rather uniform weights across the globe, typical of a first eigenvector.

This pattern is nevertheless thought to be realistic as it agrees with an analysis by Parker (7) who showed clearly the truly worldwide character of changes in global SST over most of the last 130 years. He used a "frozen grid" analysis of the SST data, much as was done by Jones et al (8) in studies of long term changes in land temperature. Parker showed that changes in data coverage did not affect conclusions about the nearly worldwide pattern of the SST changes. Note that restricted regions such as parts of the Tropical West Pacific show little long term change in SST.

EOF2 (Fig 4a) has weights concentrated in the Pacific and so may not be truly worldwide. Fig 4b shows that, not surprisingly, EOF2 is highly correlated with SST variations in the tropical E Pacific, so we can call EOF2 the "El Nino" EOF. EOF2 has little weight in the N Atlantic, where the direct effects of the "average" El Nino are known to be weak, but it clearly includes a considerable part of the extratropical N Pacific and probably the Indian Ocean where it is believed that El Nino directly affects temperature (eg Yasunari (1987) (9). EOF2 is similar to the first "global" EOF pattern of SST anomaly variation found by Hsiung and Newell (1983) (10) for the period 1949-1979 when, as Fig 3b shows, long term variations in global mean SST were weak.

Fig 5a shows the pattern of weights for EOF3; Fig 5b shows that EOF3 is quite well correlated in spring (and in summer, not shown) with Nicholson's annual Sahel rainfall index (11) updated to 1987 using CLIMAT data. (Most of the rain falls between June and October). EOF3 has weights of opposite sign in the N Atlantic (including the Mediterranean) and the S Atlantic, though the zero line is near 10°S. The Indian Ocean has weights of the same sign as those in the S Atlantic, except in a central region south of the equator, though the strongest weights are located south of 20°S. North of 40°N, the N Pacific has similar weights to those in the N Atlantic, with small weights in much of the remainder of the N Pacific. The southernmost S Pacific (S of 30°S) has similar weights to those in the extratropical S Atlantic and S Indian Ocean. Thus EOF3 seems to reflect an overall contrast in SST anomalies between the hemispheres but with rather weak signals in the tropical oceans, especially in the Pacific. EOF3 appears to be worldwide in scale but it seems that substantial areas contribute relatively little to the pattern. Following the arguments in the introduction, it is possible that the tropical weights are a little too small and the extratropical weights are a little too large in this version of EOF3.

2.2 EOFs IN INDIVIDUAL SEASONS

The calculation of seasonal EOFs from only 80 individual seasons (ie time samples) for 294 10° x 10° squares (locations) is likely to lead to sampling problems (Jolliffe, (13)). Despite these problems, the following analysis shows that EOF1 and 2 calculated in each of the four individual seasons are all similar to the equivalent "all seasons" EOFs. All seasons EOF3 is also reproduced in individual seasons but sometimes by two EOFs which, when added together, represent the all seasons EOF3 well and which, individually, are quite highly correlated with all seasons EOF3.

Table III summarises the statistical characteristics of the individual season EOFs that correspond to all seasons EOFs 1-3. EOFs 1 and 2 pass North et al's sampling test in each season except in winter, though even here the actual patterns of EOF1 and EOF2 resemble those calculated for all seasons. This is illustrated by Table IV which shows correlations (for the period 1901-80) between the time coefficient series (Z series) of all seasons EOFs 1-3 and the equivalent EOFs for individual seasons. Correlations between all seasons EOF1 and EOF1 in individual seasons are always high, the lowest value being r = 0.94 in winter and the highest r = 0.99 in spring and summer. Figs 6a and 6b show the spatial pattern of weights for EOF1 in autumn (a typical season) and the corresponding Z' time series. Note that the time series are calculated in <u>all</u> seasons even when an EOF pattern is calculated for <u>one</u> season.

High correlations are also found between all seasons EOF2 and EOF2 in the individual seasons, the lowest value again being in winter (r = .87) when North et al's test is failed. The pattern of weights for summer EOF2 and its corresponding Z' time series are shown in Figs 7a and 7b. The similarities with all seasons EOF2 (Figs 4a and 4b) are apparent. In some seasons, correlation between the seasonal EOF2 time series and Tropical E-Pacific SST becomes much poorer before about 1925, especially in winter. This may be due to data problems as substantial amounts of data had to be interpolated prior to 1925, in the Tropical Pacific.

Table IV shows that all seasons EOF3 correlates less well with corresponding EOF patterns derived for individual seasons. Only autumn passes North et al's test. In summer and winter two EOFs are almost equally well correlated with all seasons EOF3 as shown in the insert at the base of Table IV. Thus EOFs 4 and 5 in summer and EOFs 3 and 4 in winter all have correlations in the range $.7 \leq r < .8$. When their weights are added, EOFs 4 + 5 in summer correlate well with all seasons EOF3 (r= .91), as do winter EOFs 3+4 (r=.89), though the eigenvalues of these combined EOFs are distinctly larger than any of those for EOF3 alone. Only one other seasonal EOF has a correlation with all seasons EOF3 with a magnitude exceeding 0.4, (r= -0.45 for winter EOF7), so it appears that no other EOF calculated for an individual season is more than weakly related to all seasons EOF3.

Figs 8a, 8b show EOF3 for spring and a representative Z time series (for spring, March-May) plotted against annual Sahel rainfall in the same year; the correlation is weak (r=.37), considerably weaker than for all seasons EOF3 also measured in March-May (r=.59, Fig 5b). Figs 8c, 8d show EOF3 for autumn and a representative Z time series (measured in March-May) plotted against Sahel rainfall. The correlation is much stronger than for spring EOF3 (r=.57) and is similar to that with all seasons EOF3 in March-May. Overall, the seasonal EOF3 time series (or their equivalent) have similar low frequency characteristics to that for all seasons EOF3 but their interannual variability is sometimes different. It is felt that much of the variation in EOF3 (or its equivalent) is due to sampling errors. Despite this problem, the seasonal EOFs that correspond to all seasons EOF3 are significantly correlated in all four seasons to Sahel rainfall (see Table V). It must be emphasised that other 1901-80 EOFs relate to annual Sahel rainfall (Parker et al 1988) (13) so an SST pattern resembling all

seasons EOF3 is not inadequate on its own to explain or predict interannual variations in Sahel rainfall.

For completeness, Table V shows correlations between Z' time series for EOF1 calculated for the individual seasons and global mean SST. Both series are calculated in every season. Table V also shows similar correlations between EOF2 and Tropical E Pacific SST (zero lag only) and between EOF3, or its seasonal equivalent and annual Sahel rainfall in (a) March-May (b) June-August. The periods of time used for the correlations are the same as those shown in Table II. Note the similarity in the correlations between March-May or June-August Z values and annual Sahel rainfall for a given eigenvector.

3. Conclusions

This analysis shows that fairly reproducible large scale patterns of SST anomaly are found when a non-rotated covariance EOF analysis is carried out on seasonal data for all seasons together and is repeated using data in individual seasons only. However considerable sampling problems affect the analysis of individual season data so real differences between the seasons in EOF patterns of the same general shape cannot be found reliably. Sampling problems in the individual seasons might be usefully reduced by analysing SST anomalies on a 20° longitude x 10° latitude unit space scale, thereby halving the number of squares. Section 1.3 indicates that this choice is sensible because SST anomalies are better correlated in an E-W than in a N-S direction. This difference in correlation is partly but not completely due to the generally smaller dimensions of an 10° x 10° area in an E-W direction.

The all seasons EOF patterns of EOFs 1-3 are quite similar to those shown in Folland et al (1986) (14) who used slightly inferior SST data (there have been improvements in the methods of interpolating for unavailable SST data and some improvements to the 1951-80 averages and therefore to the spatial patterns of SST anomalies). It now seems that existing corrections to pre-1942 SST data may need some small but pervasive revisions whose overall effects could eventually increase the variance of EOF1. Other improvements in hand include the production of an enhanced 5° x 5° SST data set (MOHSST4) based on many millions of extra observations, mainly after 1960. A more complete perspective is also expected from the complementary use of rotated EOF analysis and the results of ongoing work on EOFs (rotated and non-rotated) of SST anomalies in individual ocean basins. In the meantime a complete set of the SST anomaly EOFs and time series described here is available from the authors on paper.

REFERENCES

1. Bottomley M., Folland C.K., Hsiung J., Newell R.E. and Parker D.E. (1988) Global Ocean Surface Temperature Atlas "GOSSTA". Joint Met Office/MIT/US Navy Project, MIT Press (in press).

2. Folland C.K. and Parker D.E. (1989) A physically based method for correcting historical sea surface temperature data. To be submitted to J. Clim. and App. Met. in autumn 1988.

3. Parker D.E. (1987) The Meteorological Office Historical Sea Surface Temperature Data Set. Met. Mag., 116, 250-254.

4. Richman M.B. (1986) Rotation of principal components. J. Climatol., 6, 293-335.

5. North G.R., Bell T.L., Cahalan R.F. and Moeng F.J. (1982) Sampling errors in the estimation of empirical orthogonal functions. Mon. Weath. Rev., 110, 75-82.

6. Bartlett M.S. (1935) Some aspects of the time-correlation problem in regard to tests of significance. J. Roy. Stat. Soc., 98, 536-543.

7. Parker D.E. (1987) The sensitivity of estimates of trends of global and hemispheric marine temperatures to limitations in geographical coverage. LRFC 12 (unpublished). Available from the Synoptic Climatology Branch, Meteorological Office, Bracknell, UK.

8. Jones P.D., Raper S.C.B., Bradley R.S., Diaz H.F., Kelly P.M. and Wigley T.M.L. (1986) Northern Hemisphere surface air temperature variations: 1851-1984. J. Clim. Appl. Met., 25, 161-179.

9. Yasunari T. (1987) Global structure of the El Nino/Southern Oscillation. Part I El Nino composites. J. Met. Soc. Japan, 65, 67-80.

10. Hsiung J. and Newell R.E. (1983) The principal non seasonal modes of variation of global sea surface temperature. J. Phys. Ocean., 13, 1957-1966.

11. Nicholson S.E. (1985) Sub-Saharan rainfall 1981-84. J. Clim. Appl. Met., 24, 1388-1391.

12. Jolliffe I.T. (1986) Principal Component Analysis. Springer Verlag.

13. Parker D.E., Folland C.K. and Ward M.N. (1988) Sea Surface Temperature anomaly patterns and the prediction of seasonal rainfall in the Sahel region of Africa. "Recent Climate Change - A Regional Approach" Ed. S. Gregory. Belhaven Press.

14. Folland C.K., Parker D.E., Ward M.N. and Colman A.W. (1986) Sahel rainfall, Northern Hemisphere circulation anomalies and worldwide sea temperature changes. LRFC 7A, unpublished, available from the Synoptic Climatology Branch, Meteorological Office, Bracknell, UK.

Table I

STATISTICAL SUMMARY OF ALL SEASONS SSTA EOFS

EOF	EIGENVALUE E	PERCENTAGE OF VARIANCE		NORTH ET AL's TEST PASSED? N
		EACH EOF	CUMULATIVE	
1	11.47	10.9	10.9	YES
2	8.19	7.7	18.6	YES
3	4.08	3.9	22.5	YES
4	3.44	3.3	25.8	YES
5	3.06	2.9	28.7	YES
6	2.72	2.6	31.3	YES
7	2.49	2.4	33.7	YES
8	2.12	2.0	35.7	NO
9	2.07	2.0	37.7	NO
10	2.04	1.9	39.6	NO

Table II

CORRELATION BETWEEN ALL SEASONS EOFS 1 TO 3 AND SELECTED TIME SERIES

	SEASONAL GLOBAL SST			
	1901-80		1856-1987	
	Z	Z'	Z	Z'
EOF 1	0.94**	0.96**	0.90**	0.92**

	SEASONAL TROPICAL E PACIFIC SST 1901-87 [10°N - 15°S, 160 W to 75 W]					
	— 1 SEASON LAG*		ZERO LAG		1 SEASON LAG	
EOF 2	Z	Z'	Z	Z'	Z	Z'
	0.59**	0.62**	0.75**	0.78**	0.68**	0.70**

	ANNUAL SAHEL RAINFALL (1901-87)			
	MARCH-MAY		JUNE-AUGUST	
EOF 3	Z	Z'	Z	Z'
	0.59*	0.57*	0.59*	0.58*

* -1 SEASON LAG IMPLIES THAT EOF 2 LEADS TROPICAL E PACIFIC SST BY 1 SEASON

** SIGNIFICANT AT 99% CONFIDENCE LEVEL (estimates only)

Table III STATISTICAL SUMMARY OF EOFS IN INDIVIDUAL SEASONS

	SPRING (March-May)				SUMMER (June-Aug)				AUTUMN (Sept-Nov)				WINTER (Dec-Feb)			
	E	P%	PC%	N	E	P%	PC%	N	E	P%	PC%	N	E	P%	PC%	N
1	12.20	11.6	11.6	YES	12.66	11.9	11.9	YES	12.85	12.8	12.8	YES	12.45	11.3	11.3	NO
2	8.81	8.4	20.0	YES	7.96	7.6	19.5	YES	10.54	10.4	23.2	YES	10.78	9.8	21.1	NO
3	4.90	4.6	24.6	NO	6.00	5.6	25.1	NO	4.94	4.9	28.1	YES	5.27)	4.8	25.9	NO
4	4.46	4.3	28.9	NO	5.19)	4.9	30.0	NO	3.65	3.7	31.8	NO	4.91)	4.5	30.4	NO
5	4.25	4.0	32.9	NO	4.07)	3.8	33.8	NO	3.28	3.2	35.0	NO	4.21	3.8	34.2	NO
6	3.85	3.7	36.6	NO	3.72	3.6	37.4	NO	3.19	3.2	38.2	NO	3.90	3.6	37.8	NO
7	3.36	3.2	39.8	NO	3.50	3.3	40.7	NO	3.04	3.0	41.2	NO	3.45	3.1	40.9	NO
8	3.10	2.9	42.7	NO	3.04	2.8	43.5	NO	2.85	2.8	44.0	NO	3.22	2.9	43.8	NO

E = eigenvalue

P% = percentage of total variance explained

PC% = cumulative percentage of total variance explained

Underlined eigenvalues are those of EOFs that correspond to all seasons EOF3

N = North et al's test - is it passed?

Table IV CORRELATION BETWEEN SST EOFS: 1901-80

	SPRING			SUMMER			AUTUMN			WINTER		
ALL SEASONS	1	2	3	1	2	4&5	1	2	3	1	2	3&4
EOF 1	0.99	(0.14)	(0.19)	0.99	(0.22)	(0.14)	0.98	(0.20)	(-0.23)	0.94	(0.39)	(0.07)
EOF 2	(0.20)	0.96	(0.08)	(-0.06)	0.95	(0.21)	(-0.04)	0.98	(0.00)	(0.37)	0.87	(-0.05)
EOF 3	(0.14)	(0.10)	0.88	(0.10)	(-0.06)	0.91	(0.11)	(0.15)	0.94	(0.21)	(-0.10)	0.89

	SUMMER 4	SUMMER 5	WINTER 3	WINTER 4
EOF 3	0.77	0.71	0.70	0.70

Table V CORRELATIONS BETWEEN INDIVIDUAL SEASONAL SST EOFs AND SELECTED TIME SERIES ALL SEASONS USED

	SEASON OF EOF PATTERN			
	WINTER	SPRING	SUMMER	AUTUMN
EOF1 Z'and GLOBAL SST 1856-1987	0.89**	0.92**	0.90**	0.90**
EOF2 Z'and TROPICAL E PACIFIC SST (zero lag) 1901-1987	0.60**	0.67**	0.80**	0.83**
EOF3+ Z in March-May and ANNUAL SAHEL RAINFALL 1901-87	0.48*	0.37	0.59**	0.57**
As above, but June-Aug 1901-87	0.43*	0.41*	0.58**	0.60**

+ EOF 4+5 in summer
EOF 3+4 in winter

** 99% Significance
* 95% Significance
(estimates only)

DIAGRAMS

Fig 1 — 10° x 10° squares used in the covariance eigenvector analysis of SST anomalies for the period 1901-80 (1951-80 averages used). Areas used are shaded.

Fig 2 — Spatial correlation of 10° x 10° SST anomalies (all seasons) in selected regions and anomalies in a central 10° x 10° square. Period used is 1901-80. Correlations are multiplied by 100.

Fig 3a — All seasons worldwide EOF1 of 10° x 10° SST anomalies 1901-80. Weights are multiplied by 1000.

Fig 3b — Z' time series of all seasons EOF1, 1856-1987. SST anomalies are weighted according to the area of the appropriate 10° x 10° square. Z' is plotted against seasonal global mean SST anomales in all seasons.

Fig 4a — As Fig 3a but EOF2.

Fig 4b — Z' time series (1901-87) of all seasons EOF2 plotted against SST anomalies observed in the tropical east Pacific defined by the area 10°N-15°S, 160°W-75°W.

Fig 5a — As Fig 3a but EOF3.

Fig 5b — Z time series of all-seasons EOF3 plotted for spring (March-May) against annual Sahel rainfall, 1901-87.

Fig 6a — EOF1 for autumn (Sept-Nov), 1901-80.

Fig 6b — Z' time series for autumn EOF1 calculated in every season and plotted against global mean SST calculated in every season.

Fig 7a — EOF2 for summer (June-August), 1901-80.

Fig 7b — Z'time series for summer EOF2 calculated in every season and plotted against global mean SST calculated in every season.

Fig 8a — EOF3 for spring (March-May), 1901-80.

Fig 8b — Z time series of EOF3 for spring plotted for spring only (March-May) versus annual Sahel rainfall, 1901-87.

Fig 8c — EOF3 for autumn (Sept-Nov), 1901-80.

Fig 8d — Z time series of autumn EOF3 plotted for spring only (March-May) against annual Sahel rainfall, 1901-87.

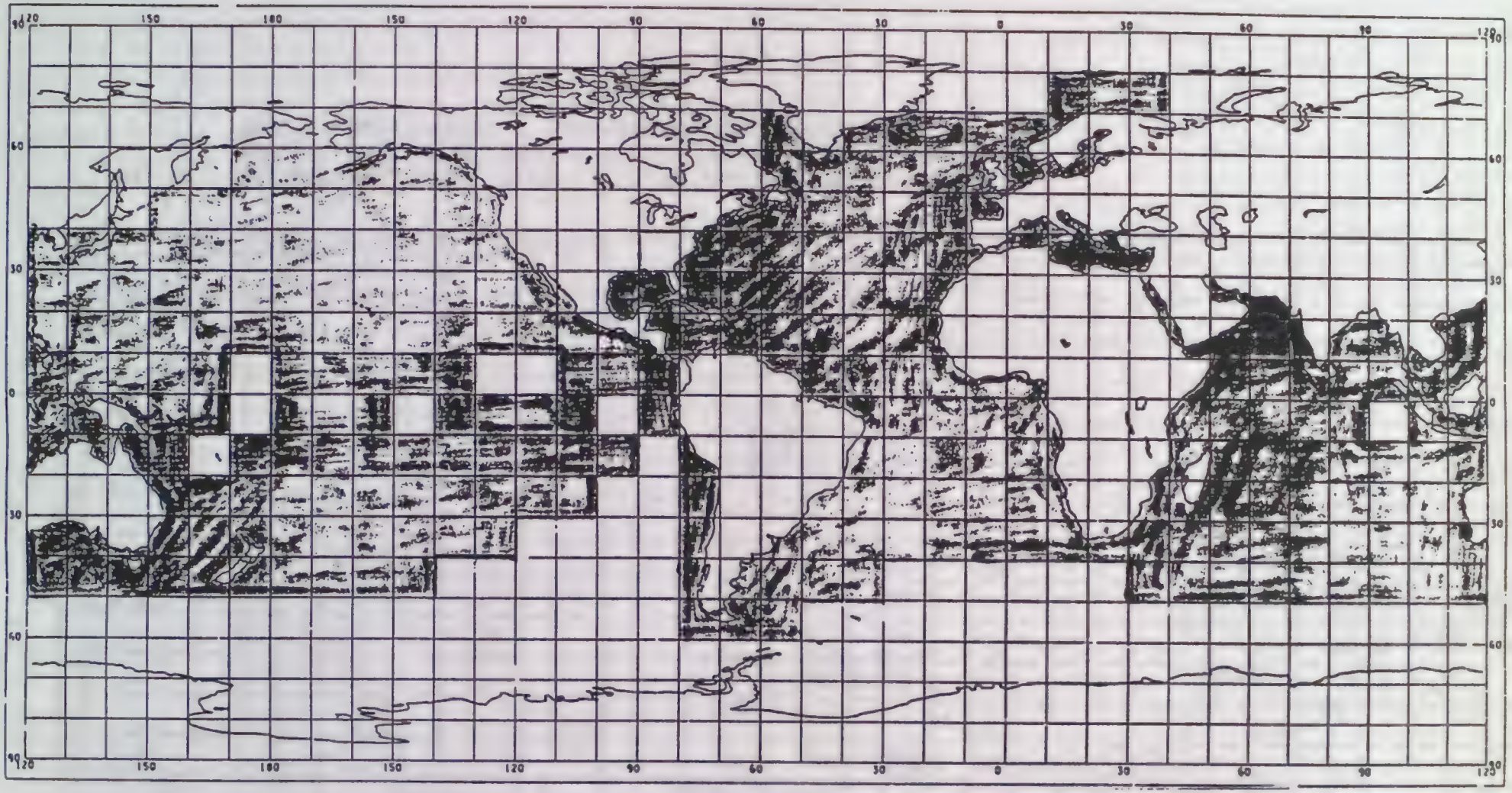

Fig 1 10° x 10° squares used in the covariance eigenvector analysis of SST anomalies for the period 1901-80 (1951-80 averages used). Areas used are shaded.

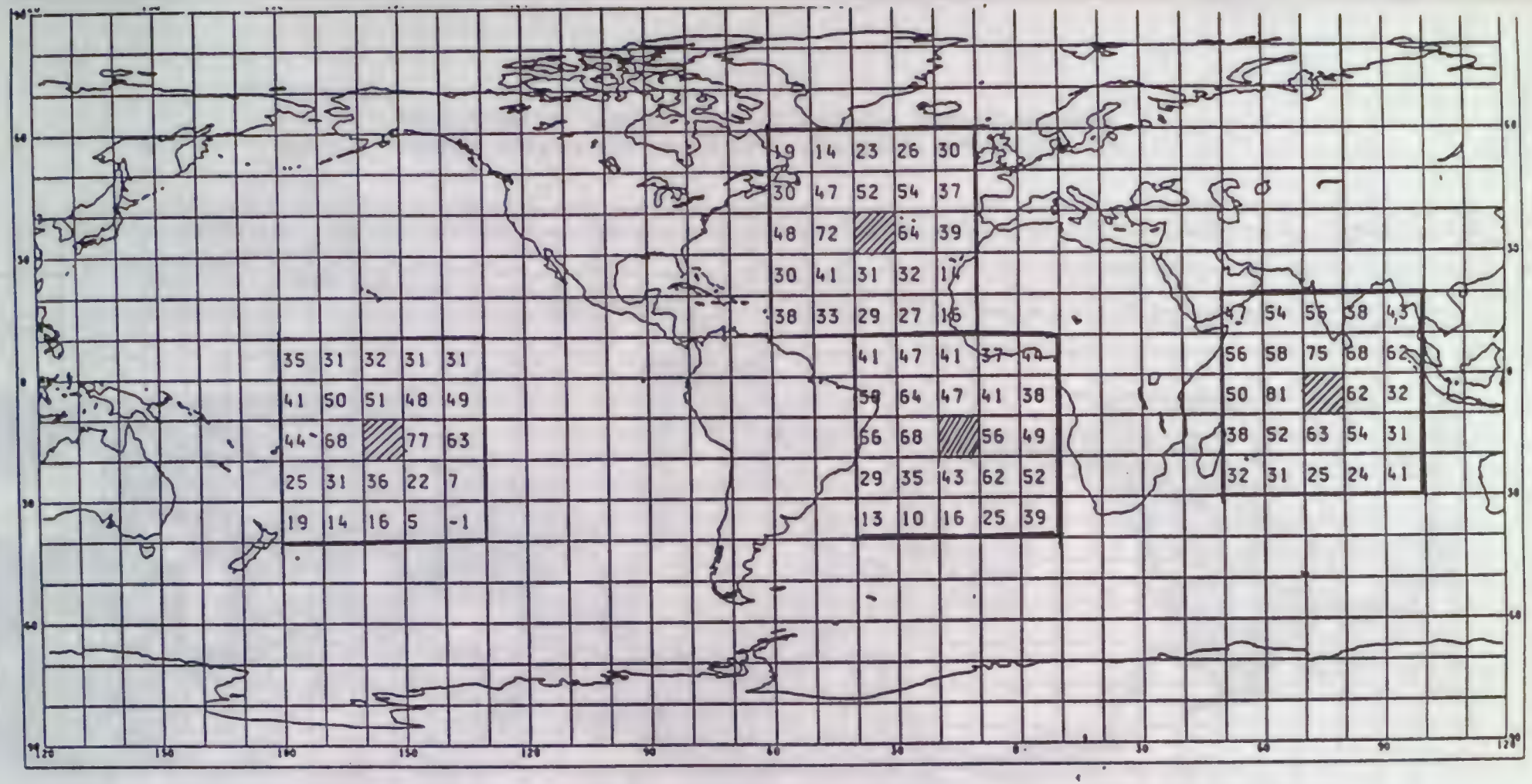

Fig 2 Spatial correlation of 10° x 10° SST anomalies (all seasons) in selected regions and anomalies in a central 10° x 10° square. Period used is 1901-80. Correlations are multiplied by 100.

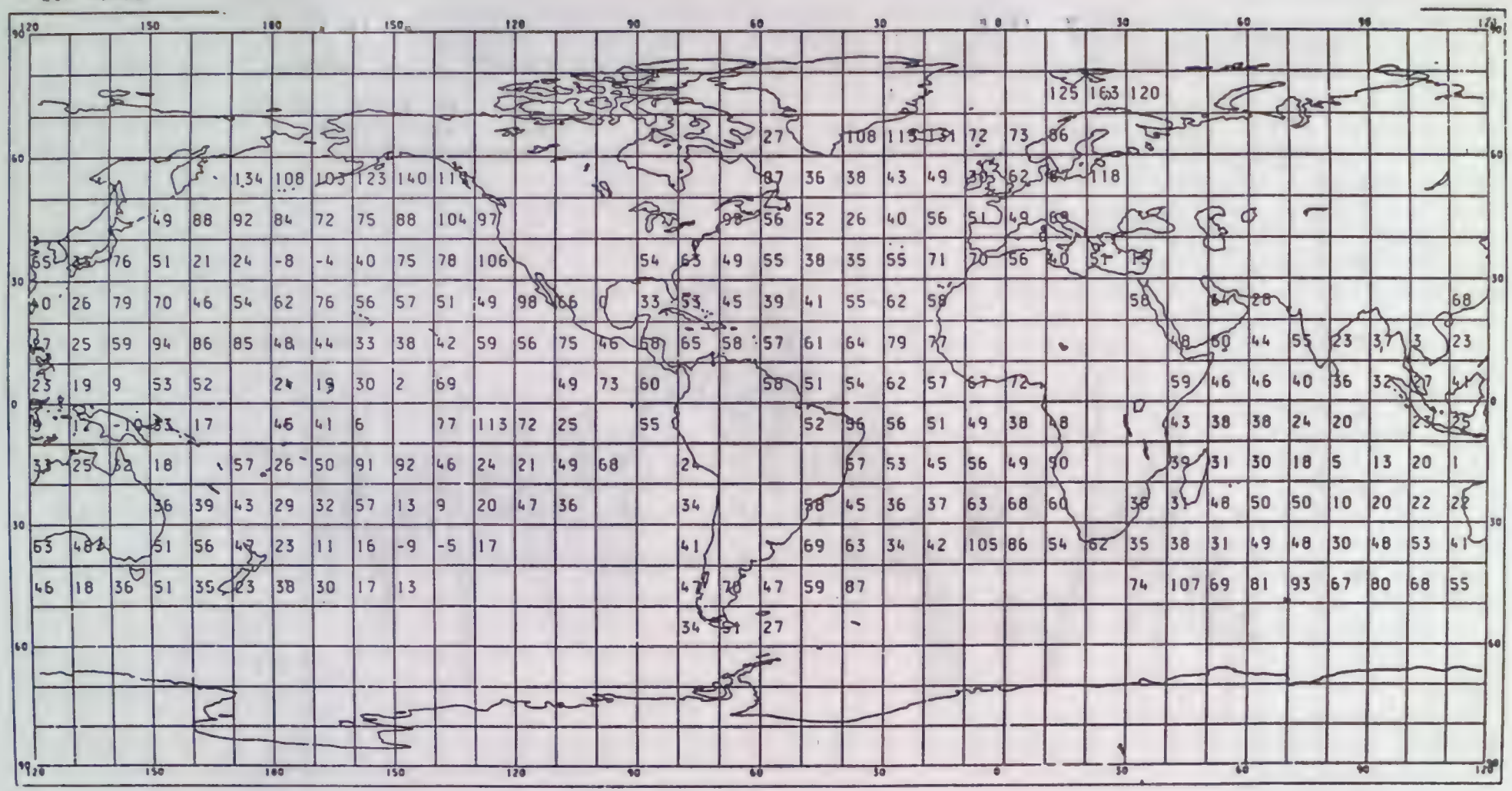

Fig 3a All seasons worldwide EOF1 of 10° x 10° SST anomalies 1901-80. Weights are multiplied by 1000.

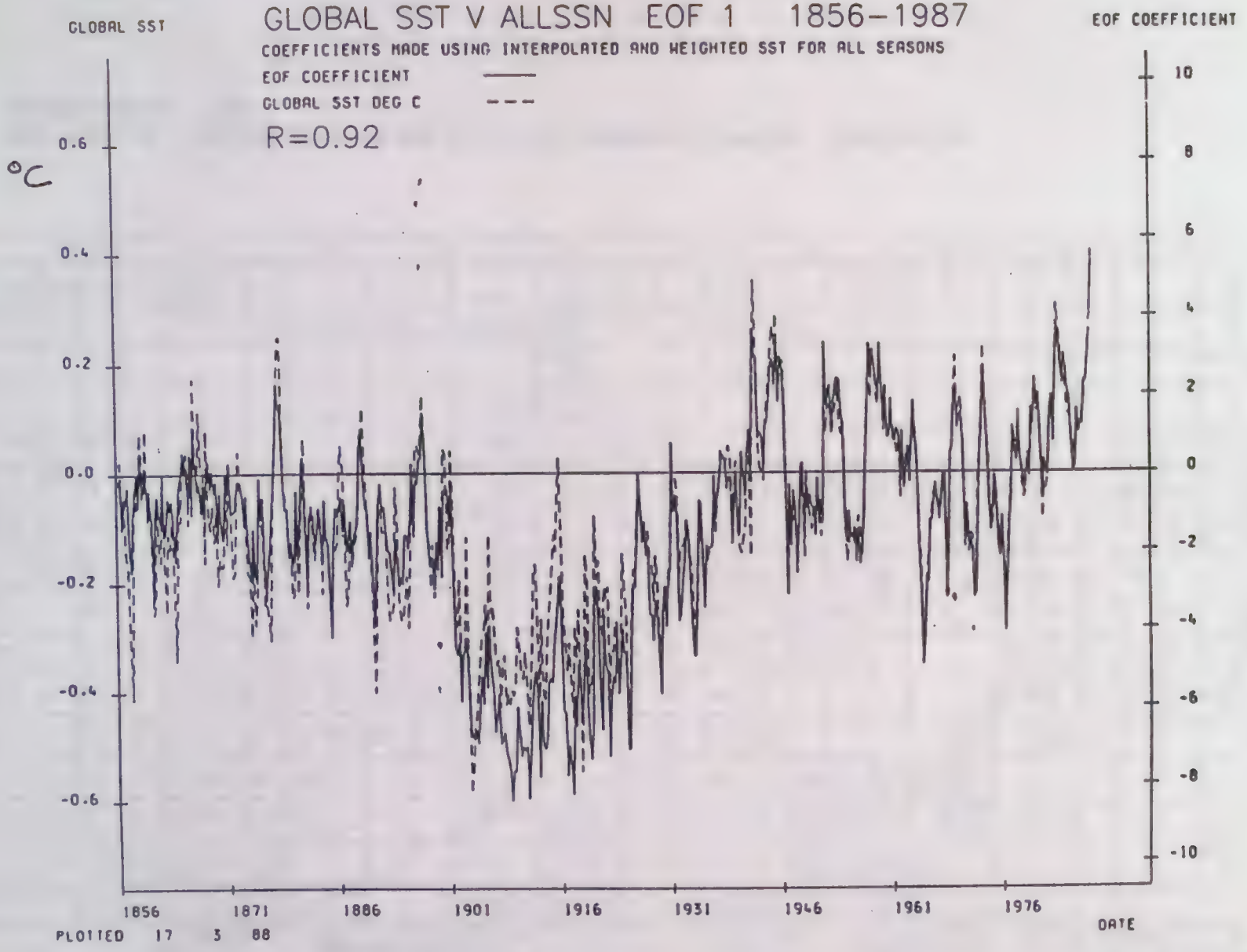

Fig 3b Z' time series of all seasons EOF1, 1856-1987. SST anomalies are weighted according to the area of the appropriate 10° x 10° square. Z' is plotted against seasonal global mean SST anomalies in all seasons

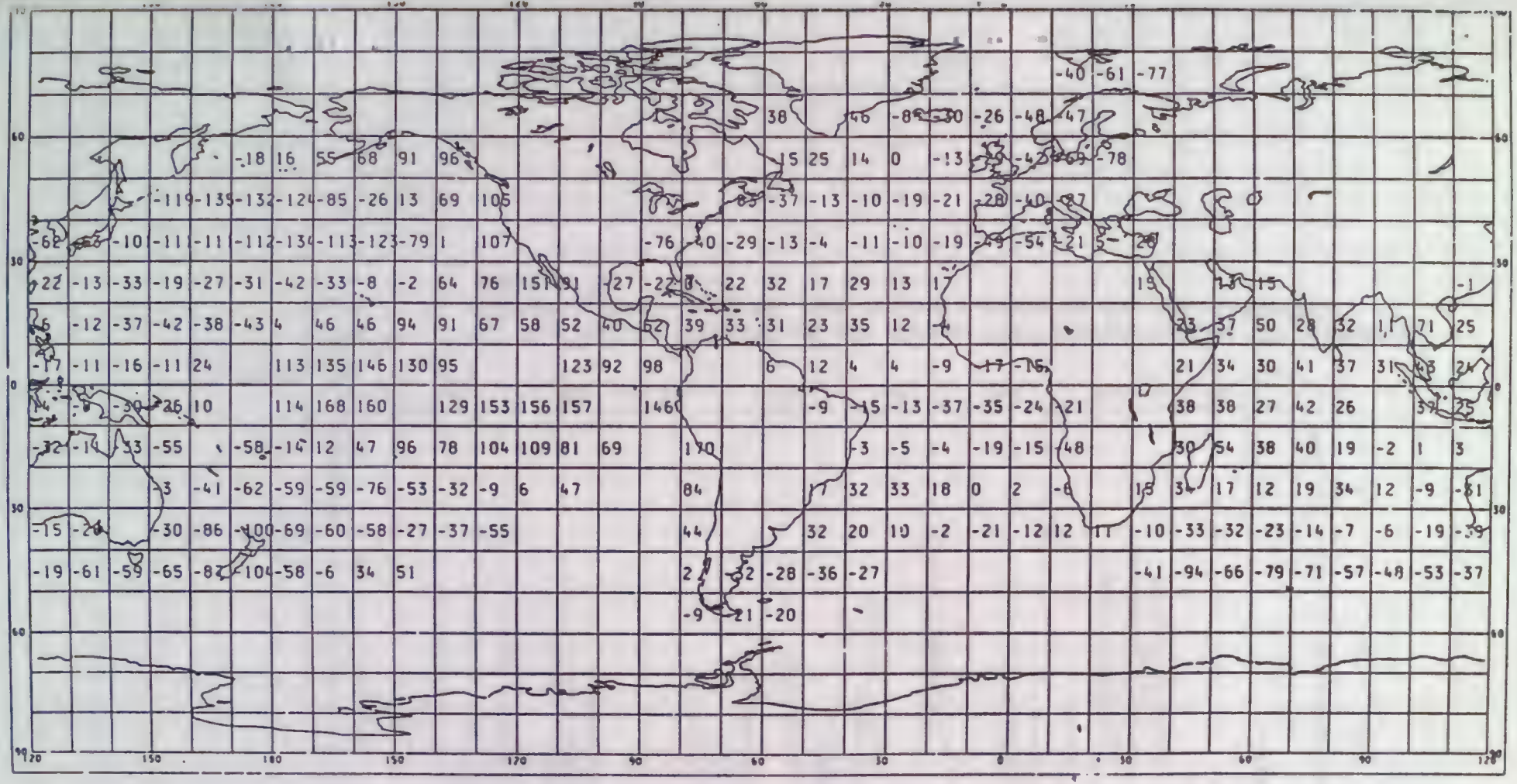

Fig 4a As Fig 3a but EOF2.

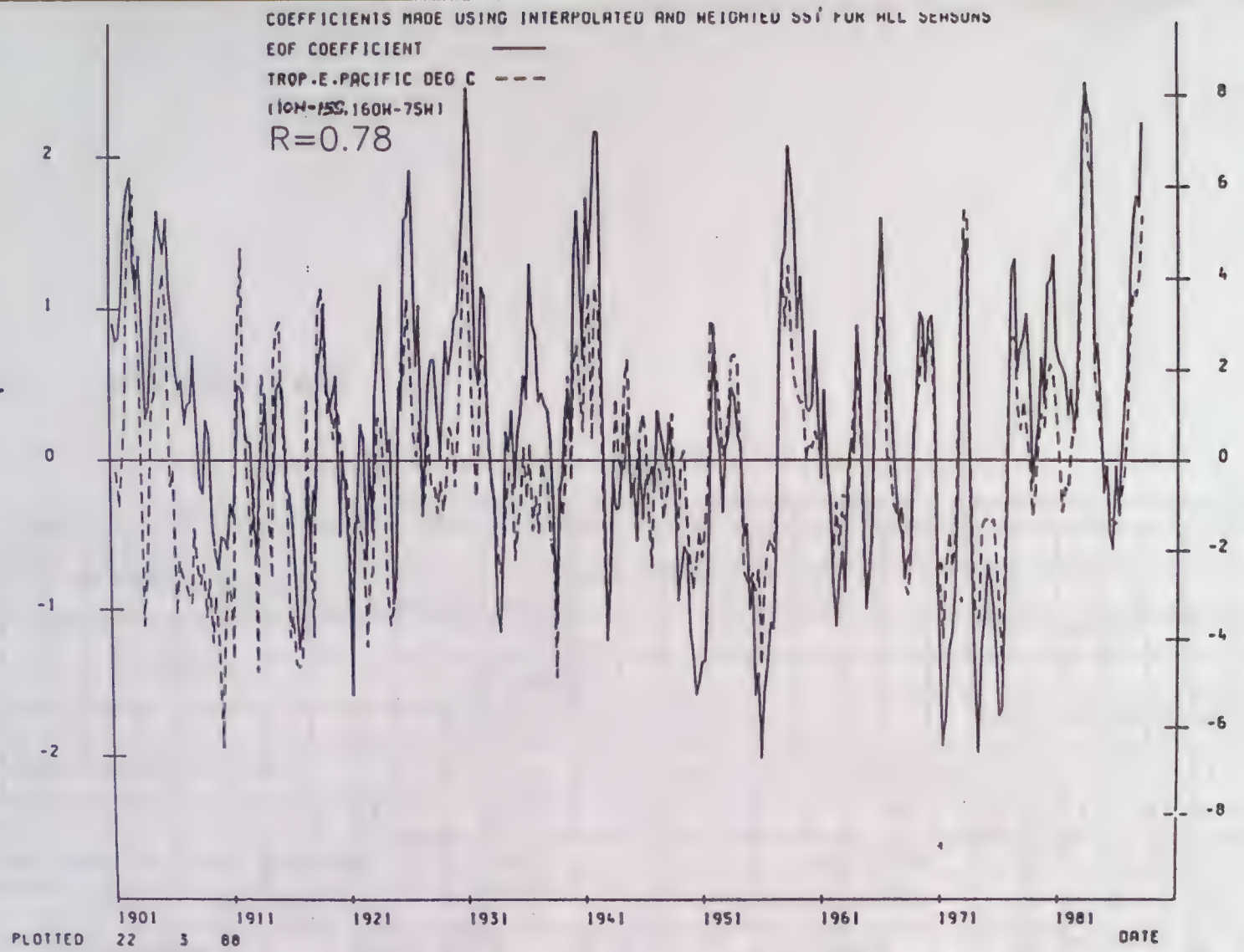

Fig 4b Z' time series (1901-87) of all seasons EOF2 plotted against SST anomalies observed in the tropical east Pacific defined by the area 10°N-15°S, 160°W-75°W.

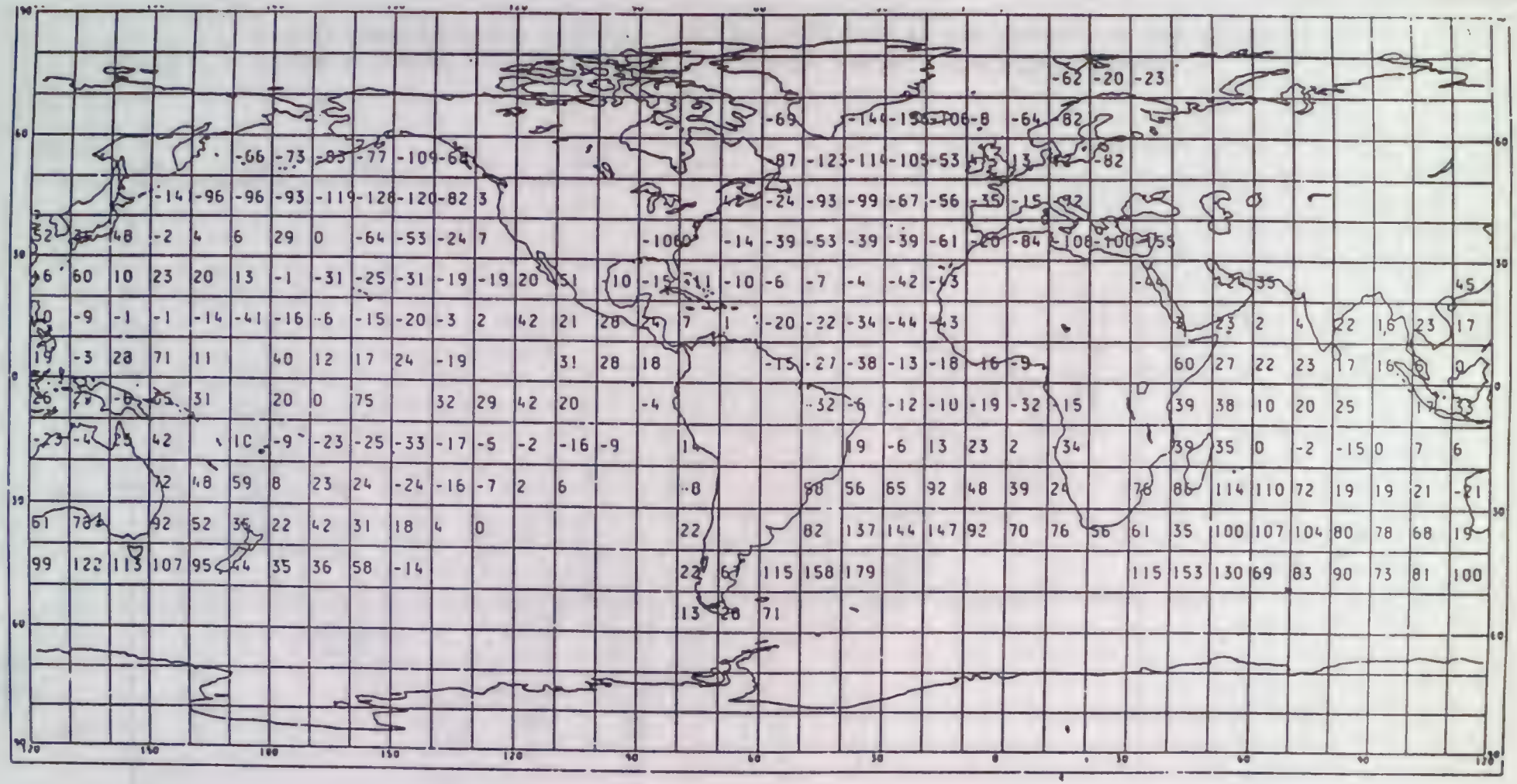

Fig 5a As Fig 3a but EOF3.

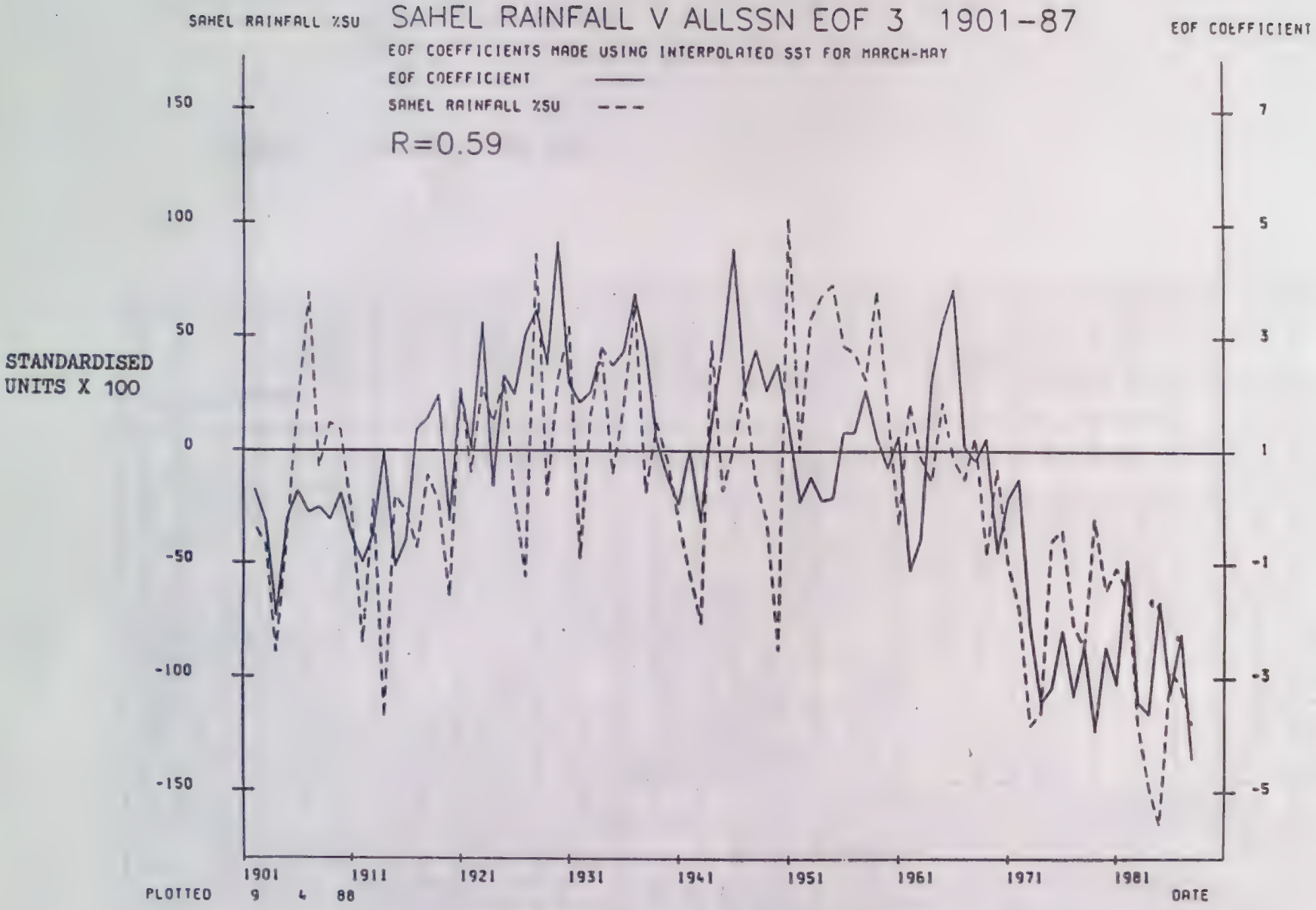

Fig 5b Z time series of <u>all-seasons</u> EOF3 plotted for <u>spring</u> (March-May) against annual Sahel rainfall, 1901-87. The EOF sign here is the reverse of that in Fig 5a.

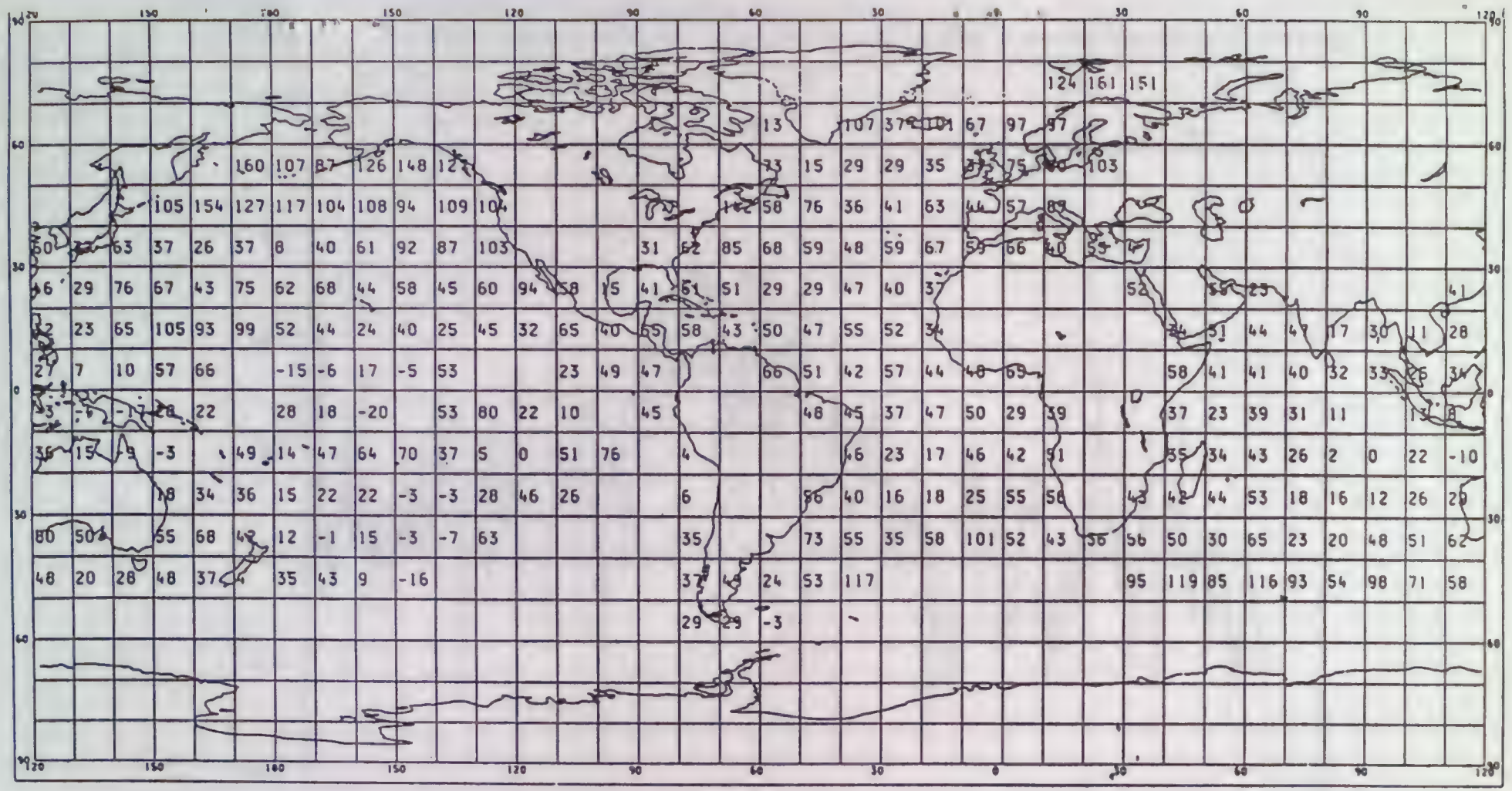

Fig 6a EOF1 for autumn (Sept-Nov), 1901-80.

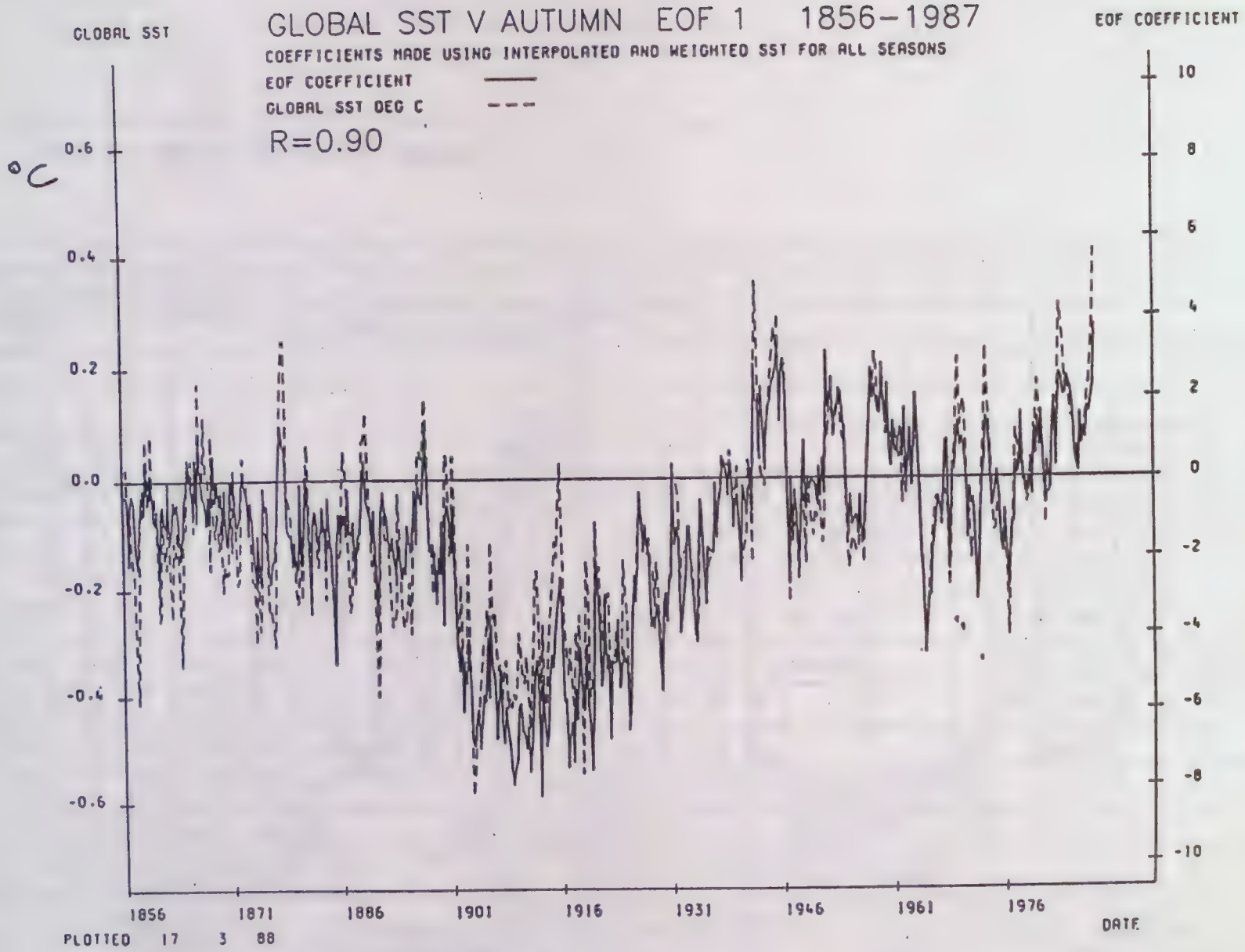

Fig 6b 'Z' time series for autumn EOF1 calculated in every season and plotted against global mean SST calculated in every season.

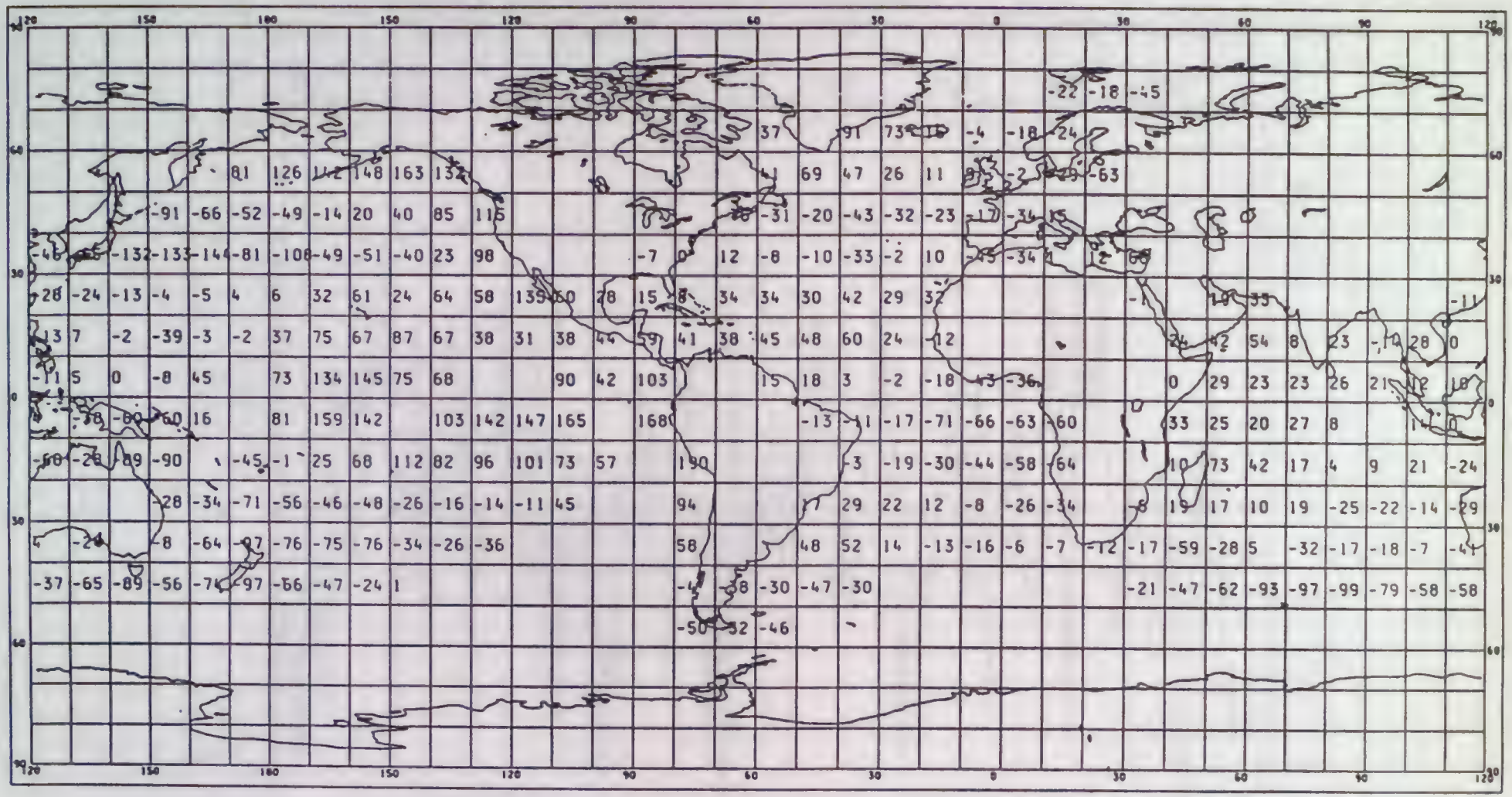

Fig 7a EOF2 for summer (June-August), 1901-80.

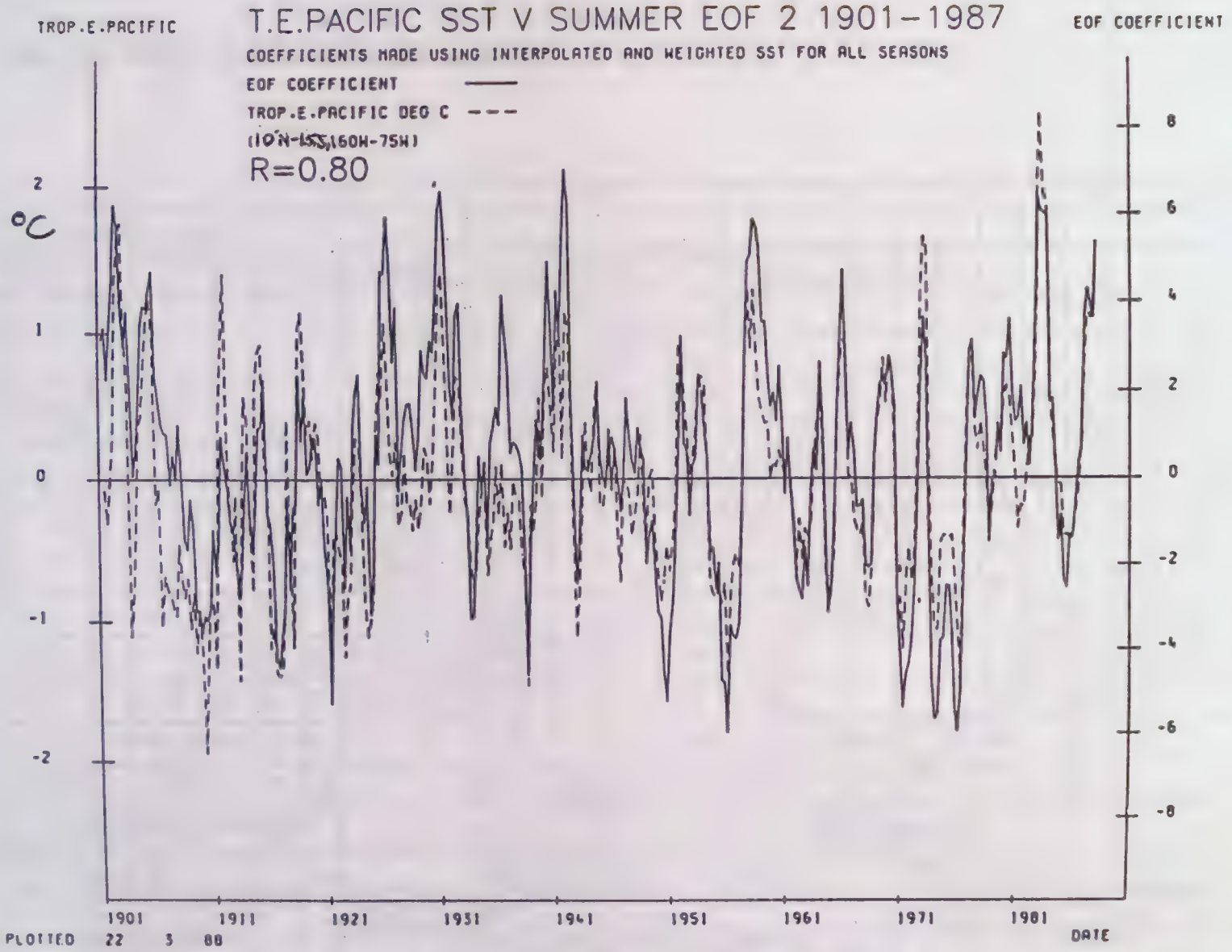

Fig 7b Z'time series for summer EOF2 calculated in every season and plotted against tropical East Pacific SST anomaly calculated in every season.

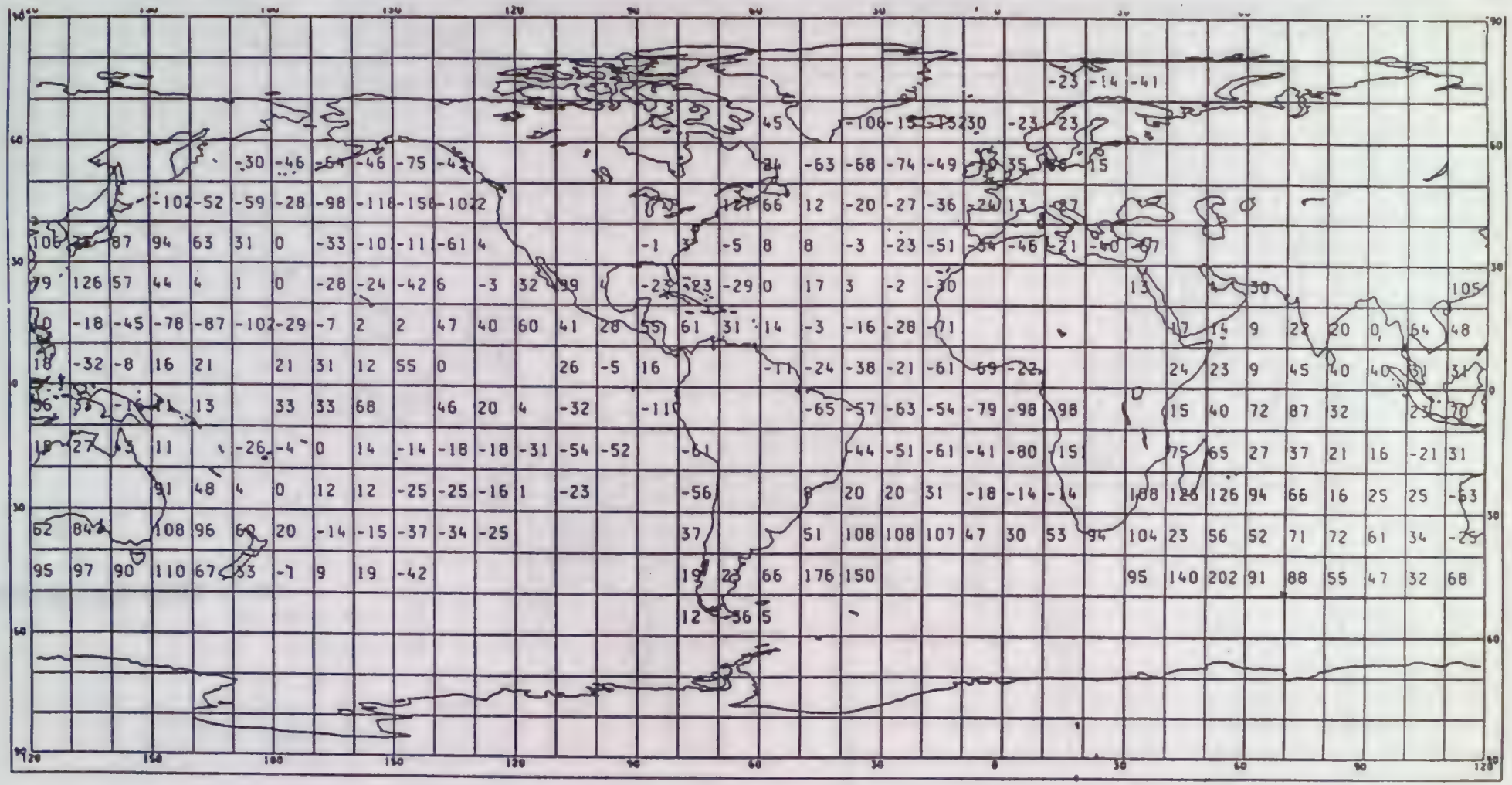

Fig 8a EOF3 for spring (March-May), 1901-80.

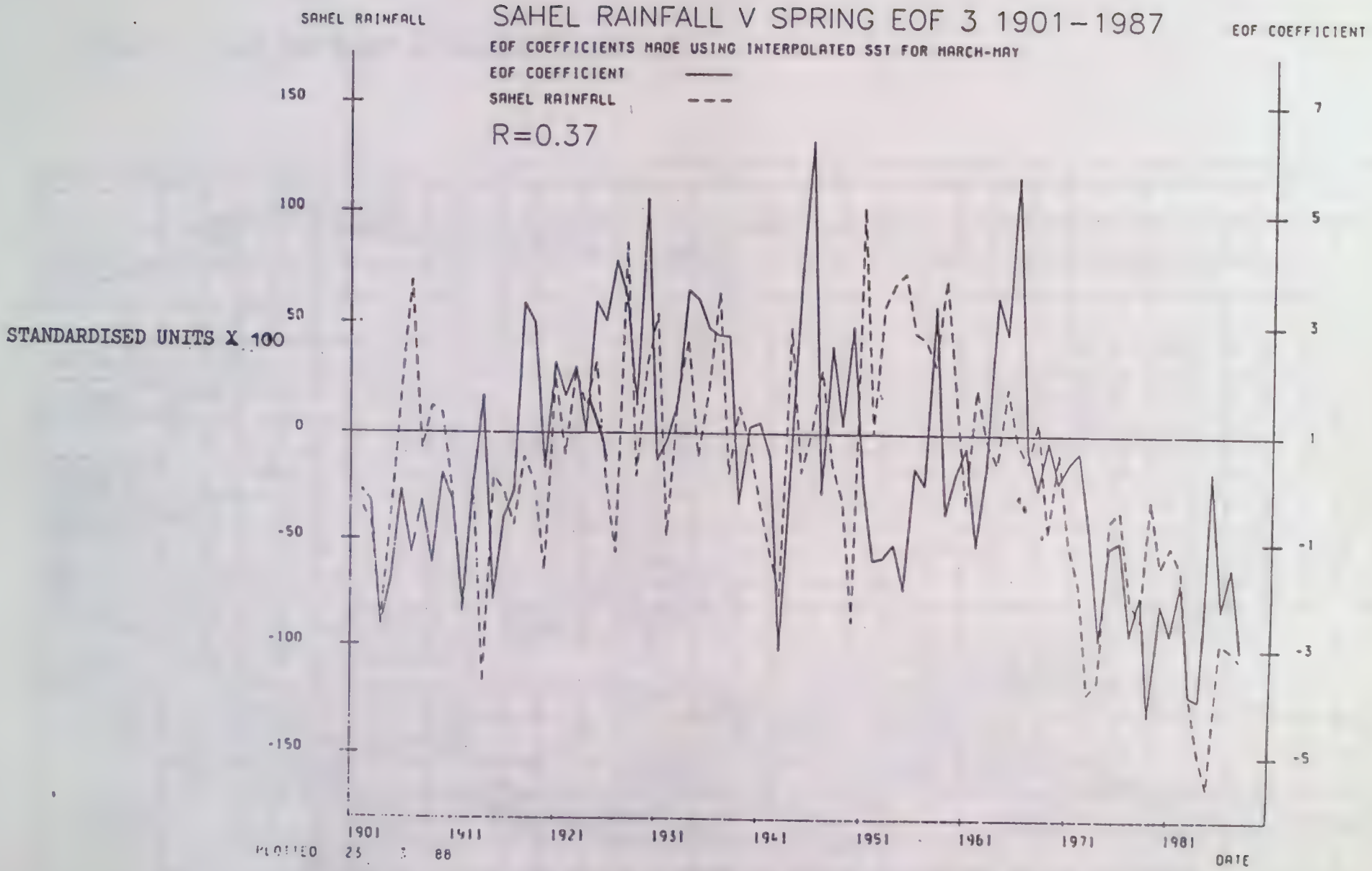

Fig 8b Z time series of EOF3 for spring plotted for spring only (March-May) versus annual Sahel rainfall, 1901-87. The EOF sign here is the reverse of that in Fig 8a.

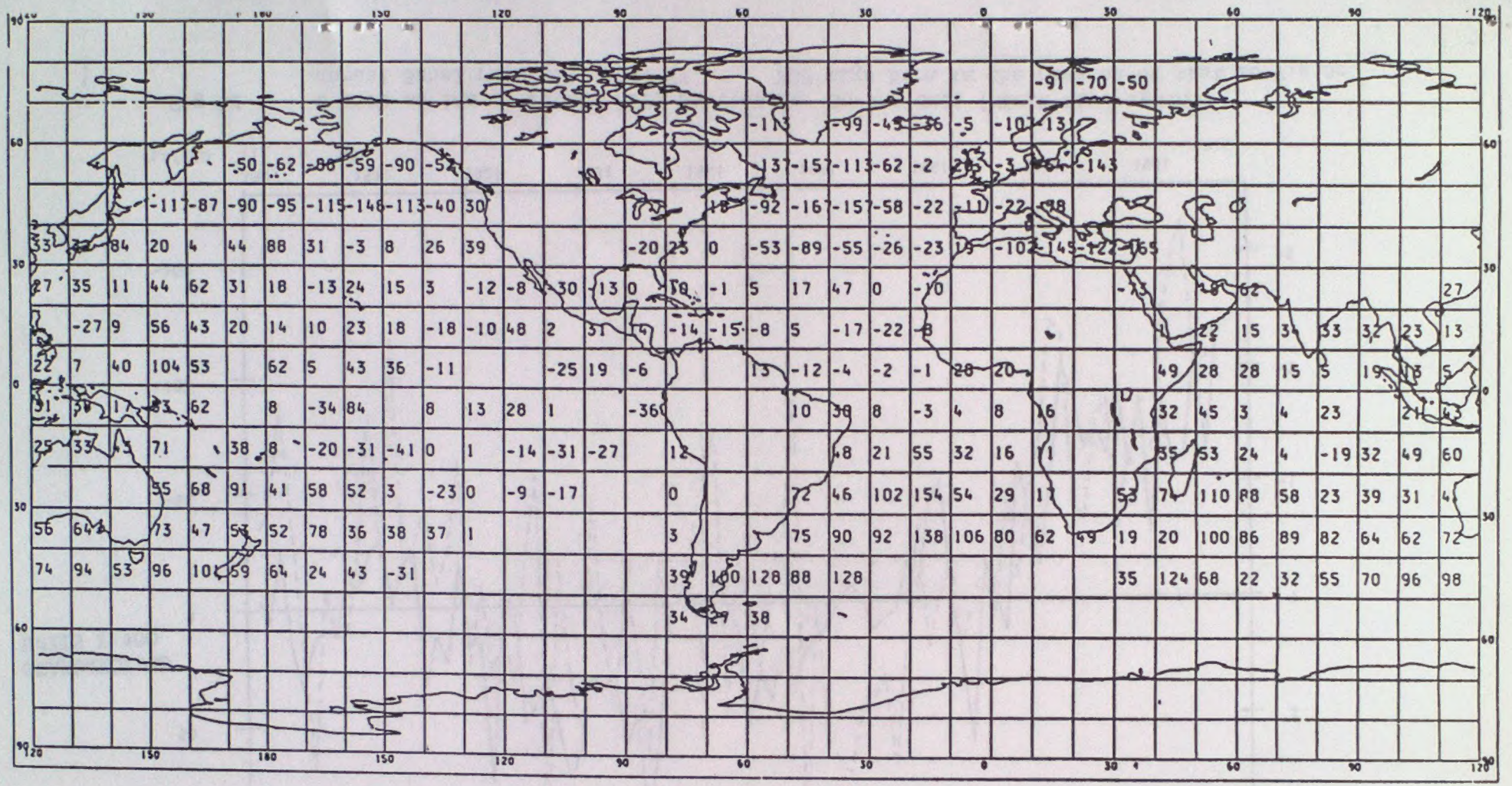

Fig 8c EOF3 for autumn (Sept-Nov), 1901-80.

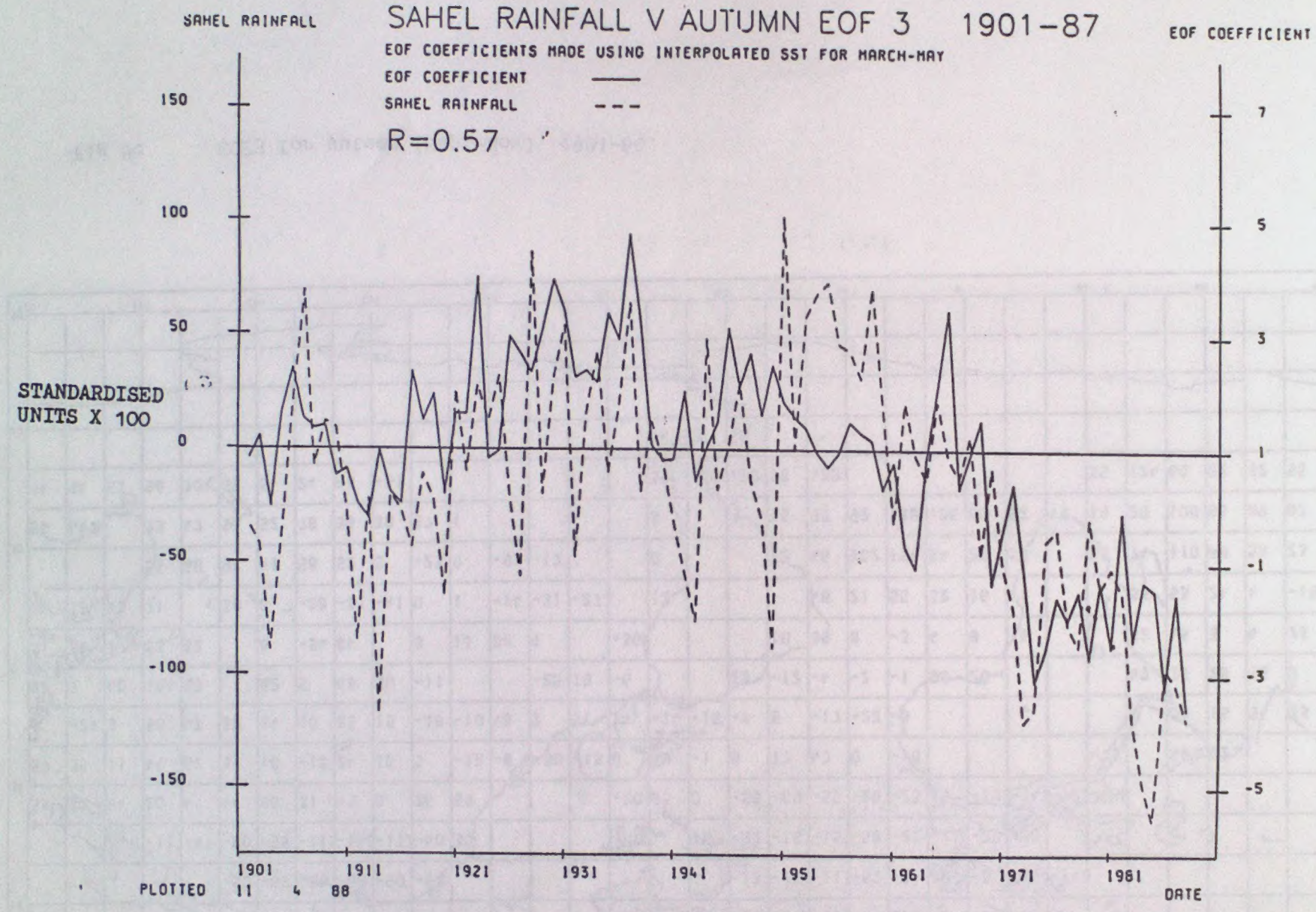

Fig 8d Z time series of autumn EOF3 plotted for spring only (March-May) against annual Sahel rainfall, 1901-87. EOF sign here is the reverse of that in Fig 8c.

INDEX TO LONG-RANGE FORECASTING AND CLIMATE RESEARCH SERIES

1) THE CLIMATE OF THE WORLD - Introduction and description of world climate.
by C K Folland (March 1986)

2) THE CLIMATE OF THE WORLD - Forcing and feedback processess.
by C K Folland (March 1986)

3) THE CLIMATE OF THE WORLD - El Nino/Southern Oscillation and the Quasi-biennial Oscillation.
by C K Folland (March 1986)

4) THE CLIMATE OF THE WORLD - Climate change: the ancient earth to the 'Little Ice Age'.
by C K Folland

5) THE CLIMATE OF THE WORLD - Climate change: the instumental period.
by C K Folland (March 1986)

6) THE CLIMATE OF THE WORLD - Carbon dioxide and climate (with appendix on simple climate models).
by C K Folland (March 1986)

7) Sahel rainfall, Northern Hempishere circulation anomalies and worldwide sea temperature changes, (To be published in the Proceedings of the "Pontifical Academy of Sciences Study Week", Vatican, 23-27 September 1986).
by C K Folland, D E Parker, M N Ward and A W Colman (September 1986)

8) Lagged-average forecast experiments with a 5-level general circulation model.
by J M Murphy (March 1986)

9) Statistical Aspects of Ensemble Forecasts.
by J M Murphy (July 1986)

10) The impact of El Nino on an Ensemble of Extended-Range Forecasts. (Submitted to Monthly Weather Review)
by J A Owen and T N Palmer (December 1986)

11) An experimental forecast of the 1987 rainfall in the Northern Nordeste region of Brazil.
by M N Ward, S Brooks and C K Folland (March 1987)

12) The sensitivity of Estimates of Trends of Global and Hemispheric Marine Temperature to Limitations in Geographical Coverage.
by D E Parker (April 1987)

13) General circulation model simulations using cloud distributions from the GAPOD satellite data archive and other sources.
by R Swinbank (May 1987)

14) Similation of the Madden and Julian Oscillation in GCM Experiments.
by R Swinbank (May 1987)

15) Numerical simulation of seasonal Sahel rainfall in four past years using observed sea surface temperatures.
by J A Owen, C K Folland and M Bottomley
(April 1988)

16) Not used

17) A note on the use of Voluntary Observing Fleet Data to estimate air-sea fluxes.
by D E Parker (April 1988)

18) Extended-range prediction experiments using an 11-level GCM
by J M Murphy and A Dickinson (April 1988)

19) Numerical models of the Raingauge Exposure problems - field experiments and an improved collector design.
by C K Folland (May 1988)

20) An interim analysis of the leading covariance eigenvectors of worldwide sea surface temperature anomalies for 1901-80.
by C K Folland and A Colman (April 1988)